Photoacclimation by Arctic Cryoconite Phototrophs

Perkins RG[1*], Bagshaw E[1], Mol L[2], Williamson CJ[3], Fagan, D[3], Gamble M[3] and Yallop ML[3]

1. Cold Climate Research, School of Earth and Ocean Sciences, Cardiff University, Park Place, Cardiff, UK, CF10 3AT

2. Department of Geography and Environmental Management, UWE Bristol, Coldharbour Lane, Bristol, UK, BS16 1QY

3. School of Biological Sciences, Life Sciences Building, University of Bristol, 24 Tyndall Avenue, BS8 1TQ

*Corresponding author: Email: PerkinsR@cf.ac.uk, Tel.: 0044 (0)2920 875026

Abstract

Cryoconite is a matrix of sediment, biogenic polymer and a microbial community which resides on glacier surfaces. The phototrophic component of this community is well adapted to this extreme environment, including high light stress. Photoacclimation of the cryoconite phototrophic community on Longyearbreen, Svalbard was investigated using in situ variable chlorophyll fluorescence. Rapid light curves (RLCs) and induction recovery curves were used to analyse PSII quantum efficiency, relative electron transport rate and forms of down regulation including non-photochemical quenching (NPQ) including state transitions in cyanobacteria. Phototrophs used a combination of behavioural and physiological photochemical down regulation. Behavioural down regulation is hypothesised to incorporate chloroplast movement and cell or filament positioning within the sediment matrix in order to shade from high light, which resulted in a lack of saturation of RLCs and hence over-estimation of productivity. Physiological down regulation was biphasic NPQ: comprising a steadily induced light-dependent form and a light-independent NPQ that was not reversed with decreasing light intensity. These findings demonstrate that cryoconite phototrophs combine multiple forms of physiological and behavioural down regulation to optimise light exposure and maximise photosynthetic productivity. This plasticity of photoacclimation enables them to survive productively in the high light stress environment on the ice surface.

Keywords: cryoconite, photoacclimation, down regulation, non-photochemical quenching, productivity, fluorescence

Introduction

Cryoconite (cryo = ice, conite = dust) is an important component of the glacier ecosystem. It consists of debris deposited on the ice surface by wind, water, or rockfall from valley sides, and collects in water-filled pools on the surface known as cryoconite holes. The debris contains microorganisms, including photoautotrophs, which contribute to the accumulation of carbon and bioavailable nutrients on glacier surfaces (Hodson *et al.* 2007; Cook *et al.* 2012; Bagshaw *et al.* 2016a). These nutrients are periodically exported to downstream environments via glacier runoff (Bagshaw *et al.* 2010; Lawson *et al.* 2014), and can support biological activity in proximal ecosystems (Foreman *et al.* 2004; Bagshaw *et al.* 2013). Microorganisms in cryoconite are typically sourced from the surrounding environments, and include cyanobacteria, microalgae, archaea, bacteria, fungi and heterotrophic protists (Cameron *et al.* 2012; Edwards *et al.* 2014; Zawierucha *et al.* 2015; Kaczmarek *et al.* 2016). It is well-established that the photosynthetic organisms are active throughout the ablation season, but the mechanisms by which they undertake primary production on the harsh environment of the glacier surface are poorly understood. In this paper, we use in situ variable chlorophyll fluorescence to investigate cryoconite community photophysiology in order to gain insight into their adaptation to high light intensity, 24 h photoperiods (and hence the resulting high photodose) and rapid light intensity fluctuation.

Glacier surface microorganisms have been demonstrated to impact on ice surface albedo (Takeuchi 2002b; Yallop *et al.* 2012; Musilova *et al.* 2016), via a phenomenon known as ‘biological darkening’ (Benning *et al.*, 2014; Tedesco *et al.* 2016). In and ex situ studies have demonstrated that this occurs via two mechanisms: production of organic matter, which has a net darkening impact on the sediment (Takeuchi 2002a; Musilova *et al.* 2016), and production of dark pigments (Yallop *et al.* 2012; Lutz *et al.* 2014; Remias *et al.* 2016), which serve to protect photosynthetic apparatus from high light and/or UV (Dieser *et al.* 2010).

Yallop *et al.* (2012) demonstrated that highly pigmented populations of algae are widespread in marginal zones of the Greenland ice sheet, both concentrated in cryoconite, and living directly on the ice surface. Within cryoconite holes, the material aggregates into granules, forming a matrix of sediment particles and the microbial community, bound with biogenic extracellular polymers (EPS) (Hodson *et al.* 2010; Langford *et al.* 2010; Zarsky *et al.* 2013). These tightly-knit granules give structure to the cryoconite community, with heterotrophic organisms concentrated in the centre and phototrophs around the outside, which promotes community stability on the constantly changing glacier surface. During the summer months, cryoconite is regularly redistributed by flowing meltwater (Irvine-Fynn *et al.* 2011), hence granule formation may be an adaptation to promote community longevity (Bagshaw *et al.* 2016b).

To our knowledge there have been very limited in situ measurements of microbial phototrophs in ice/snow-associated communities, presumably due to the difficulty in collecting data in these harsh environments. McMinn *et al.* (2007) used variable chlorophyll fluorescence to perform measurements on ex situ samples of Antarctic sea ice algae. Stibal *et al.* (2007) used in situ variable chlorophyll fluorescence to measure snow algae, however these samples were thawed and analysed in a cuvette system. Yallop *et al.* (2012) investigated ice algal photophysiology and their role in reducing ice sheet albedo, but samples were analysed ex situ after thawing. Bagshaw *et al.* (2016) made a comparative study of Arctic and Antarctic cryoconite using combined oxymetry and fluorescence, also on ex situ cryoconite material in a cuvette system. By contrast, this is the first study of cryoconite phototroph photophysiology in situ. We use a Walz Water PAM flourometer with fibre optic emitter-detector to perform in situ rapid light response curves and induction recovery curves in cryoconite holes on Longyearbreen, Svalbard, in order to understand the role of photophysiological down regulation in optimising primary production in this extreme environment.

Methods

In situ field measurements and sampling

Field work was carried out at Longyearbreen, Svalbard (78° 10 49 N, 15°30 21 E) in the high-Arctic, on 25-30th August 2015. Longyearbreen is a small (2.5km^2), thin (53m, (Langford *et al.*, 2014)), predominantly cold-based valley glacier, adjacent to the town of Longyearbyen, surrounded by Tertiary and Cretaceous sandstone (Larsson 1982) interbedded with coal-bearing shales and siltstones (Langford *et al.* 2014). Field observations indicate that sediment production is driven by frost shattering of the bedrock and glacial action. This material is moved onto the glacier surface through aeolian deposition and high frequency rock falls (Etzelmüller *et al.* 2011).

Sampling was undertaken near the centre line of the glacier (Figure 1), which had relatively high debris concentrations including a small morainic deposit. Three hydrologically connected cryoconite holes were chosen at random within 10 m^2 at 78°10.903 N, 15°31.469 E, for in situ measurements and sample collection for identification of the photosynthetic community structure using microscopy and pigment analysis. Sediment depth was 4-6 mm and water depth was 10-15 mm in the three holes.

Bulk samples of cryoconite from each hole were collected immediately after fluorescence measurements were made (see below), using new nitrile gloves and Whirlpak sterile sampling bags (Fisher Scientific). They were frozen within 4 hours of collection, and transported frozen in insulated boxes to Cardiff University, UK. Samples for initial microscopy were scraped from the debris or ice surface using an ethanol-sterilised knife or spatula, and transferred to new centrifuge tubes. They were returned to the field laboratory, kept cool and examined within 48 hours. During the short sampling period, incoming photosynthetically available radiation (PAR) and water temperature of an example cryoconite hole in the sampling area were monitored using an Apogee Quantum sensor and Campbell Scientific 107 probe, powered by a Campbell Scientific CR10X datalogger.

In situ variable chlorophyll fluorescence measurements were made using a Walz Water Pulse Amplitude Modulated (PAM) fluorometer equipped with a blue light fibre-optic emitter/detector unit. This instrument measures emitted fluorescence yield for calculation of photosystem II (PSII) quantum efficiency, which in turn can be used to calculate relative electron transport rate as a proxy for photophysiological productivity. Measurements consisted of 10 rapid light curves (RLCs) and 5 induction-recovery curves within each cryoconite hole, carried out over the same time period each day, between approximately 10:00 and 18:00 when solar irradiance was high. The photoperiod at the time of sampling in August 2015 was 20 h. Initially three measurements of RLCs were made with a blue or a red light emitter/detector unit to investigate the relative excitation of microalgae and cyanobacteria respectively (this was prior to identification of taxa present, however cyanobacteria were expected based on previous work and literature). However, no significant difference was observed between the two systems and therefore measurements were only made with one, the blue light emitter/detector unit. RLCs were in two forms: increasing and decreasing incremental light steps, with 5 replicates of each, following the methods of Perkins *et al.* (2006). Increasing and decreasing light curves were carried out on separate samples each time and with sequentially increasing or decreasing light levels steps respectively. Increasing eight-step RLCs were carried out using 30 second incremental light steps between 0 and 3,600 µmol m^{-2} s^{-1} photosynthetic available radiation (PAR). A 600 mS saturating pulse at intensity setting 10 (in excess of 8,000 µmol m^{-2} s^{-1} PAR) was observed to induce full light saturation and rise to maximum fluorescence yield (F_m or F_m'). The increasing incremental light curves were randomly interspersed with 5 replicates of decreasing incremental light curves. For these light curves, instead of using the pre-programmed RLC settings of the fluorometer, manual light curves were performed, decreasing the light intensity each step using Walz WinControl V3.14 software. At the end of each light curve step a saturating pulse was performed and the light level reduced to the next lower intensity, culminating in a 30 second dark period measurement. Rapid light curves of relative electron transport rate (rETR) as a function of incremental light intensity were plotted, with rETR calculated as:-

$$\text{rETR} = \text{quantum efficiency } (\Delta F/F_m') \times \text{PAR}/2$$

where $\Delta F/F_m'$ is the quantum efficiency calculated as $(F_m'-F)/F_m'$ and where F is the operational fluorescence yield and F_m' is the maximum fluorescence yield in the light and $\Delta F = F_m' - F$. RLC data were analysed by iterative curve fitting of the Eilers and Peeters (1988) model using Sigmaplot V10 statistical software. Light curves data were solved to determine the RLC parameters of relative maximum electron transport rate ($rETR_{max}$), light utilisation coefficient (α), and light saturation coefficients (E_s and E_k). Light curve coefficients a, b and c and the regression fit for the light curves were all observed to be significant at $p < 0.001$ ensuring accuracy in calculation of the light curve parameters (Perkins *et al.* 2006). Parameters $rETR_{max}$, α, Ek and Es were analysed for equal variance and normality using the Levene's and Shapiro Wilkes tests respectively in PAST statistical software (Hammer *et al.*, 2001). Data were homoscadestistic and parametric; two factor ANOVA was used to determine significant differences between the three cryoconite holes and between increasing and decreasing RLCs. RLC *in situ* measurements were performed randomly between the three cryoconite holes over two days, with induction recovery curves performed the following day. Again, 5 sets of measurements were performed for each cryoconite hole.

Induction recovery curves consisted of an initial dark measurement (30 seconds of darkness) of quantum efficiency (F_v/F_m), followed by a 400 second induction phase of applied actinic light at 803 µmol m^{-2} s^{-1} PAR, with repeated recording of quantum efficiency ($\Delta F/F_m'$). This was then followed by the recovery phase of a further 900 seconds of darkness, with repeated measurement of quantum efficiency (F_v/F_m). Changes in quantum yield and fluorescence yields (operational fluorescence yield F, and maximum fluorescence yields F_m and F_m') were analysed over the full induction-recovery period.

Community analysis

Cells in cryoconite subsamples were identified using a Leica DM LB2 light microscope with fluorescence attachment. For pigment quantification, subsamples of cryoconite material, frozen (-20°C) were freeze-dried and homogenised prior to the extraction of a known mass (circa 2 g) and pigments were extracted in 100% acetone containing vitamin E as the internal standard. The HPLC protocol was a modified version of the method of Van Heukelem & Thomas (2001), using a c8 column in an Agilent 1100 HPLC equipped with a diode-array detector. Pigments were identified and quantified against analytical standards from DHI and Sigma using both retention time and spectral analysis.

Results

Ambient photosynthetically available radiation (PAR) received on the glacier surface ranged from 200 to 400 µmol m^{-2} s^{-1} (st dev. 18) during the measurement period. The mean water temperature in the monitored cryoconite hole was 0.9 °C, and ranged from 0.4 to 1.9 °C. The sampled holes remained hydrologically connected throughout the monitoring period, although the degree of connection varied diurnally. The sediment layers remained intact, nonetheless mobile sediment particles were observed moving across the ice surface in the meltwater (Irvine-Fynn *et al.,* 2011).

Cryoconite phototrophic community composition

Epifluorescence microscopy on cryoconite material revealed the presence of a number of different green algal and cyanobacterial taxa in the three different cryoconite holes sampled (Table 1). Large colonies of *Nostoc* spp. (Figure 2a) and Streptophytes (closely related to Charophyceae and Embryophyta), were identified in samples from all three holes. Pigments characterising both green algae and cyanobacteria were recorded from the cryoconite material using HPLC (Table 2). Chlorophyll *a* (CHL *a*) pigment dominated all samples, but was higher in hole 1 than holes 2 and 3. Hole 1 also had the highest concentrations of the pigments lutein (LUT), chlorophyll b (CHL b) and echinenone (ECHI)). The ratios of Lutein and CHLb : CHL *a* (Table 3) were 2-6 times greater than in the other samples, indicating that green algae dominated the community in this hole. There were two key cyanobacterial markers, echinenone (ECHI) and canthaxanthin (CANT) present in all samples from the three cryoconite holes. The orange-brown pigment Scytonemin (present in the sheath of *Nostoc* (Figure 2a)) was found in all samples though it could not be quantified due to poor resolution of the peaks. Although occasional spores of *Chlamydomonas* spp. were found (Figure 2c), the red pigment astaxanthin was below the detection limit in pigment extracts. Detectable levels of fucoxanthinin holes 1 and 3, indicated that diatoms were also present. Differences in the ratios of pigment markers between holes indicated differences in relative abundance of taxa, with relatively more cyanobacteria in hole 1.

Cryoconite phototrophic community photophysiology

Increasing rapid light curves (RLCs) showed virtually no saturation (Figure 3), with 14 of 15 curves failing to saturate, and one single curve approaching saturation. As a result,

$rETR_{max}$ could only be estimated as the highest value obtained (255 ± 37.2 rel. units). In contrast, decreasing RLCs (Figure 3) showed clear saturation, with all 15 curves saturating and an $rETR_{max}$ of 113 rel. units ($F_{2,10}$ = 551, p<0.001). Hence, $rETR_{max}$ determined from decreasing RLCs was less than 50% of the value estimated from the non-saturating, increasing RLCs. Examination of both sets of RLCs showed no significant difference in the light saturation coefficient (α), with values of 0.13 (increasing) and 0.12 (decreasing) rel. units. For decreasing RLCs, an E_k of 940 and E_s of 1800 µmol m^{-2} s^{-1} PAR, were determined.

Calculated down regulation in the form of non-photochemical quenching (NPQ) was notably different between increasing and decreasing RLCs (Figure 4); note that calculated values do not correct for NPQ retained from the period prior to measurements, i.e. induced under ambient light. For decreasing RLCs there was no initial dark light curve step, and hence no reversal of any NPQ that had been induced under ambient light prior to the measurement period. Whilst NPQ slowly increased with PAR from 0 to 0.50 ± 0.06 during increasing RLCs, an inverse relationship between NPQ and PAR was apparent during decreasing curves: as light levels were stepped down from 3505 to approximately 800 µmol m^{-2} s^{-1} PAR, NPQ slowly increased. With further reductions in PAR, NPQ rapidly increased to approximately 6-times that induced during increasing RLCs. These high levels of NPQ were further retained in the dark during the final 30 second step of decreasing RLCs.

Examination of RLC fluorescence yields revealed the dynamics underlying observed differences in down regulation between increasing and decreasing RLCs (Figure 5). During increasing RLCs (Figure 5a), initial increases in both F and F_m' signified reversal of NPQ retained from illumination of samples by ambient light prior to measurements: such retained NPQ was reversed under the initially low PAR levels of increasing RLCs. As samples were subjected to increasing light intensity, F_m' decreased steadily to 84 ± 23.2% of initial values due to NPQ induction, whilst F' returned to approximately initial values (103 ± 29.3% of the value in the dark). Conversely, both *F'* and F_m*'* slowly decreased below initial values (measured in the dark, F_o and F_m) at the beginning of decreasing RLCs (Figure 5b), with decreases accelerating at light intensity less than ca. 800 µmol m^{-2} s^{-1}, the point at which NPQ increased. With decreases in light intensity to 140 µmol m^{-2} s^{-1}, *F'* reduced to 53 ± 9.9% and F_m*'* to 64 ± 11.4% of initial values. Note the slight increase in both *F'* and F_m*'* when exposed to darkness at the end of decreasing RLCs (Figure 5b).

Monitoring of photochemistry during induction/recovery curves indicated a small amount of photoacclimation during the 400-second induction phase at 803 µmol m^{-2} s^{-1}, whereby initial declines in quantum efficiency from 0.29 ± 0.025 to 0.11 ± 0.038 at the onset of illumination were recovered to 0.13 ± 0.025 by the end illumination (Figure 6). With the onset of the dark recovery phase, rapid increases in quantum efficiency to 0.26 ± 0.041 demonstrated almost full recovery to initial values. During the remainder of the recovery phase, quantum efficiency slowly increased to 0.45 ± 0.063, i.e. well above initial values, suggesting significant retention of down regulation in samples from exposure to ambient light prior to measurements. However, examination of the operational (*F'* or *F* in the induction and recovery phases, respectively) and maximum (F_m*'* or F_m, respectively) fluorescence yields (Figure 7) revealed unexpected patterns. *F'* initially increased during the induction phase, presumably due to ubiquinone Qa reduction (lack of increase in F_m*'* precluding NPQ relaxation), before decreasing as Qa oxidation (unlikely) and/or NPQ induction (most likely) occurred during the induction phase. After 400 seconds, decreases in *F* with the onset of the dark recovery phase, presumably reflecting Qa oxidation, outweighed the effects of NPQ reversal; however, continued decreases in *F* over the remainder of the recovery phase suggested continued NPQ induction in darkness. In a similar manner, F_m*'* decreased during the induction phase suggesting NPQ induction, showed a slight increase with the onset of the recovery phase, i.e. slight NPQ reversal, though subsequently declined over the remainder of the recovery phase indicating continued NPQ induction in the dark. Increases in quantum efficiency during the recovery phase (Figure 6) were the result of a greater proportional decrease in F compared to F_m (Figure 7).

Discussion

Cryoconite phototrophs on Longyearbreen, Svalbard demonstrated a high capability for rapid photoacclimation, via a combination of behavioural and physiological down regulation of photochemistry. The former involves a self-shading process, either chloroplast shading, cell positioning within the cryoconite sediment, or both processes. The latter appears to be a combination of two forms of non-photochemical quenching (NPQ), however this is complicated as a result of the mixed community due to employment of state changes by cyanobacteria which induce rapid changes in fluorescence yields in the same form as NPQ. Overall, there is a high plasticity of photoacclimation in croconite phototrophs, which ensures cells are ideally adapted to high light exposure on the ice surfaces in these high-stress polar environments.

The phototrophic communities of the three cryoconite holes investigated clearly differed despite being hydrologically connected. Pigment analysis indicated that all three holes showed the typical dominance of green algae and cyanophyta within cryoconite material (Langford *et al.*, 2011; Cameron *et al.*, 2012; Yallop *et al.*, 2012; Edwards *et al.*, 2014), with only trace levels of fucoxanthin and hence low biomass of diatoms. Hole 1 was dominated by green algae, principally chlorophytes and streptophytes (indicated by high Chl b : Chl a ratio and the relatively high presence of lutein; streptophytes are closely related to Charophyceae and Embryophyta and hence have similar pigments), whereas holes 2 and 3 were relatively more dominated by cyanobacteria. The cyanobacteria community also differed between holes, based on the relative concentrations of echinenone and canthaxanthin, although all three holes had a high relative abundance of *Nostoc*. Interestingly, there were no significant differences in community measurements of photophysiology between the holes, despite the differences in phototrophic community structure.

Photophysiological data from rapid light curves and induction/recovery curves demonstrated a high plasticity of response, with several mechanisms of photoacclimation identified that allow the cryoconite phototrophic community to effectively photoacclimate to the high-light regime experienced *in situ*. Photoacclimation methods can be considered to be either physiological or behavioural (Perkins *et al*. 2002; 2010a,b; Lavaud and Goss 2015). Physiological photoacclimation refers largely to photochemical down regulation, including non-photochemical quenching (NPQ) in eukaryote phototrophs, whereby the light-driven de-epoxidation of specific xanthophyll pigments quenches excess excitation energy in the antennae complex as heat (Consalvey et al. 2005; Lavaud and Lepetit 2013). In cyanobacteria, state transitions to balance excitation between photosystems is also a form of physiological photochemical regulation (Campbell et al. 1998). Behavioural photoacclimation is largely cell motility as a response to changes in light environment, whereby cells move away from high light or towards low light in order to optimise their efficiency of photochemistry (Forster and Kromkamp 2004; Perkins *et al*. 2002; 2010a,b). However, Yallop *et al.* (2012) expanded upon this by hypothesising that ice algae used chloroplast movement to facilitate shading behind dark, tertiary pigments. Separation of the two processes through in situ measurements would be extremely difficult, if not impossible, hence we refer to behavioural down regulation as the likely composite of these two processes. We therefore hypothesise that cryoconite phototrophs utilise chloroplast movement and / or cell positioning in order to adjust to changing light environments. Such cell motility to facilitate shading within the cryoconite matrix likely explains why light curves with increasing light increments failed to saturate, whereas decreasing light curves did saturate. Increasing curves provide enough time for chloroplast movement inside the cells and/or cell or filament movement in the sediment and hence the cells optimise their light environment. Phototrophic cryoconite communities are organised around granule structures, consisting of mineral grains, microorganisms and polymers (Takeuchi *et al.* 2001; Hodson *et al.* 2010; Langford *et al.* 2010; Segawa *et al.* 2014). This is analogous to microbial biofilms in fine sediments, where down regulation is achieved using a mixture of cell motility and NPQ (Perkins *et al.* 2010a,b; Lavaud and Goss 2015). In these systems, a lack of RLC saturation has been attributed to cell movement away from increasing light levels (Perkins *et al.* 2002; 2010a,b). Cyanobacteria, green algae and diatoms are known to utilise cell motility to move away from high light and UV-stress through the process of microcycling and bulk migration (Bebout and Garcia-Pichel 1995; Kromkamp *et al.* 1998; Consalvey *et al.* 2004; Forster and Kromkamp 2004; Serôdio 2004; Perkins *et al.* 2002; 2010a,b). During the present study, microscopy and pigment profiles confirmed the presence of cyanobacteria, diatoms (at very low levels of abundance) and green algae in the cryoconite material, corroborating previous findings (Stibal *et al.* 2006; Yallop and Anesio 2010), and hence supporting the potential of cell motility as a means of down regulation. Cell movement within sediment is usually facilitated by extracellular polymer production (Consalvey *et al.* 2004), which is a well-reported characteristic of cryoconite granules (Langford *et al.* 2010; Zarsky *et al.* 2013; Segawa *et al.* 2014). Granules promote community stability (Hodson *et al.* 2010; Irvine-Fynn *et al.* 2011; Langford *et al.* 2014; Bagshaw *et al.* 2016b), and as we now reveal, also play a role in behavioural photoacclimation, Aggregation of cryoconite into granules thus enhances community production, by supporting a stable, cooperative microbial community, enabling physical migration to cope with the extreme glacier surface environment.

Behavioural down regulation of photochemistry (chloroplast movement and / or cell positioning within the sediment) has therefore been demonstrated for cryoconite phototrophic communities, but what is the role of physiological down regulation (in the form of NPQ in green algae and diatoms and state transitions in cyanobacteria) for these phototrophs? Calculation of NPQ from the change in maximum fluorescence yield during increasing incremental RLCs, indicated an initial reversal of NPQ retained from exposure to ambient light prior to measurements, highlighting NPQ as an important mechanism of down-regulation employed by cryoconite communities in situ. The subsequent slow induction of NPQ to values of around 0.5 during increasing RLCs further suggested this form of down-regulation to be applied proportionally to irradiance, as is a commonly held assumption underlying NPQ dynamics in microalgae (e.g. Lavaud and Goss 2014). However, by extending our assessment to include both decreasing light curves and induction/recovery curves, we were able to demonstrate unique features in the dynamics of cryoconite community down regulation that would not have been ascertainable using the commonly-applied increasing light curve technique alone. Firstly, contrasting dynamics in down-regulation during increasing and decreasing light curves indicated that behavioural, as opposed to physiological, down-regulation may form the major photo-acclimation mechanism employed in cryoconite holes on Svalbard glaciers. This would be in agreement for observations on sediment biofilm communities in intertidal estuaries (Perkins et al. 2010a,b; Cartaxana et al. 2011). This is evidenced by the six-fold higher induction of NPQ apparent during decreasing as compared to increasing light curves, although the true magnitude difference in NPQ induction should not be directly compared, due to the differential levels of cell movement hypothesised. Cell movement to induce shading would result in a decrease in F_m' yield as well as that observed due to induction of NPQ (Forster and Kromkamp, 2004, Perkins et al., 2010), thus confounding the measurement of NPQ based on change in maximum fluorescence yield (see Methods). Thus high NPQ could in fact be the sum of true NPQ induction and cell movement both reducing F_m' yield. However it is highly likely that the observed patterns in NPQ are indeed primarily physiological down regulation (energy dependent down regulation in eukaryote microalgae, but also state transitions in cyanobacteria, see below), at least in decreasing RLCs due to the timing and rate of induction. As well as demonstrating the significantly higher capacity for NPQ available to cryoconite phototrophs than estimated from increasing light curves, these trends provide insight into the likely balance between behavioural and physiological down-regulation employed in situ. During increasing light curves, it is likely that chloroplast movement and/or cell positioning in the sediment matrix, i.e. behavioural down-regulation, reduced the light stress experienced by cells, therefore reducing the requirement to induce NPQ. In contrast, the initial high light stress experienced during decreasing curves, coupled with the lack of time for chloroplast movement and/or cell positioning, resulted in cells inducing physiological down-regulation, i.e. NPQ, as a means to balance the irradiance provided. By comparing the magnitude of NPQ induced with/without the presence of behavioural down regulation, data indicate that the latter may account for ca. 75 % of the total down-regulation employed in cryoconite holes. In eukaryote microalgae this may be an adaptation to reduce the metabolic costs associated with production and inter-conversion of NPQ-associated pigments (Lavaud and Goss 2014) in this high-light environment. Secondly, the contrasting dynamics in down-regulation observed during the present study strongly indicated that additional to a combination of behavioural and typical physiological forms of down regulation, the cryoconite phototrophic communities further possess a rapidly induced, time or light-dose dependent form of NPQ, as opposed to primarily light intensity driven forms. With the onset of decreasing light curves, an initial slow level of NPQ was induced, followed by a more rapid induction at light levels below 800 μmol m^{-2} s^{-1} PAR. This would parallel the different forms of NPQ reported for diatoms (Lavaud and Goss 2014), although diatoms were observed to have extremely low abundance in the cryoconite. Rapidly induced energy dependent down regulation of this form, which is not reversed in darkness has been reported (Lavaud and Lepetit 2013) and referred to as photoinhibitory quenching (qI) or saturating NPQ (NPQs). NPQ was induced rapidly during our experiment, despite decreasing light levels, and was also retained in the dark. Such trends were also apparent during the dark recovery phase of induction/recovery curves. Examination of the fluorescence yields showed that both F and F_m initially increased in the dark recovery phase, presumably due to NPQ reversal, but then declined despite the increase in dark quantum efficiency (F_v/F_m) observed. There would therefore appear to be either a time or potentially light-dose dependent form of physiological down-regulation that, once triggered, does not decrease with decreasing PAR, nor is rapidly (i.e. within the duration of dark recovery employed here) reversed in the dark.

It is important to note that our measurements were made on a mixed community largely dominated by green algae and cyanobacteria. The latter appear not to have energy dependent NPQ but rapid changes in fluorescence are observed through state transitions utilising phycobilosome diffusion (Campbell and Oquist 1996, Campbell et al. 1998). This form of rapid down regulation would result in similar changes in fluorescent yields as NPQ in green algae, e.g. a quenching as light increased followed by reversal in darkness. During increasing rapid light curves, state transitions (state 2 to state 1) would result in a decrease in F_m' and hence an increase in our measured NPQ, however shading processes through cell motility described above would negate the need for this down regulation in increasing RLCs. In decreasing light curves, state 2 to state 1 transition would be induced in cyanobacteria at the same time as energy dependent NPQ would be induced in the eukaryote microalgae. It may be that as light levels reduced in these decreasing RLCs, the induction of this state transition was not reversed increasing the relative level of quenching and hence the large increase in measured NPQ. Obviously it would not be possible to differentiate between the two processes in such a mixed community using in situ fluorescence measurements, however we suggest that there is a high likelihood of physiological down regulation employed by both the eukaryote microalgae (energy dependent down regulation) and cyanobacteria (state transitions).

The combination of chloroplast movement, cell positioning and physiological down regulation by the cryoconite phototrophs is a highly efficient method of light acclimation that has serious implications for the interpretation of fluorescence based assessments of productivity. Specifically, the lack of saturation of light curves with increasing light increments indicates caution is required when utilising fluorescence on cryoconite. Productivity ($rETR_{max}$) can clearly be significantly over-estimated when photoacclimation during the light curve occurs, whether this is through cell movement or chloroplast shading. In this study, the first steps of the RLC appear to be relatively unaffected, with α similar for increasing and decreasing RLCs. However, as the light curves progressed, divergence between the curves showed an overestimation of $rETR_{max}$ of over 100%, with similar over-estimation likely for light saturation parameters E_s and E_k. This should be corrected for in studies using fluorescence in order to avoid overestimation of productivity, and potentially the role of cryoconite phototrophs in carbon flux calculations (Hodson *et al.* 2007; Anesio *et al.* 2010; Cook *et al.* 2012; Chandler *et al.* 2015; Bagshaw *et al.* 2016a).

In conclusion, this study demonstrates that the phototrophic cryoconite community on Longyearbreen, Svalbard, utilise a mixture of behavioural and physiological (likely a mixture of non-photochemical quenching in eukaryotes and state transitions in cyanobacteria) down regulation of photochemistry. Cells appear to be capable of optimising their light environment through chloroplast shading and/or cell positioning within the cryoconite, effectively behavioural down regulation. Shading through chloroplast movement and cell positioning is likely to result in an overestimation of productivity when using increasing incremental rapid light curves. In future work this may me corrected for by using the product of ETR and the operational fluorescence F' (Ihnken et al. 2014), however this was tested in this study and did not alter the shape of the RLCs. In the cryoconite studied here, the phototrophs, primarily a mixture of green algae and two different cyanophyte communities, showed high plasticity of photophysiology, indicating extremely high capability for light acclimation. This would be expected for cells inhabiting polar ice surfaces, where light intensity and light dose can be high and fluctuate quickly. Aggregation of cryoconite into granules is therefore an important adaptation which not only prolongs microbial community stability, but also allows light acclimation and hence promotes ecosystem productivity.

Acknowledgements

RP was funded by a British Phycological Society Small Project Grant. LM had combined funding from Royal Geography Society Small Research Grant, Geological Society of London Robert Scott Memorial Award and Forskningsradet Norge, Arctic Field Grant no 246072. The work was carried out on Research Project RiS 10281. MLY was supported by a Leverhulme Research Fellowship RF 2014-708. We should also like to thank the two anonymous reviewers for their highly constructive reviews.

References

Anesio, AM., Sattler, B, Foreman, CM., Telling, J, Hodson, A, Tranter, M and Psenner, R. Carbon Fluxes through Bacterial Communities on Glacier Surfaces. Annals of Glaciology 2010; 51(56): 32-40

Bagshaw, EA, Tranter, M, Fountain, AG, Welch, K, Basagic, HJ and Lyons, WB . Do Cryoconite Holes Have the Potential to Be Significant Sources of C, N, and P to Downstream Depauperate. Arctic Antarctic and Alpine Research 2013; 45(4): 440-454 doi: 10.1657/1938-4246-45.4.440

Bagshaw, EA, Tranter, M, Wadham, J, Fountain, AG, Dubnick, A and Fitzsimons, S . Processes Controlling Carbon Cycling in Antarctic Glacier Surface Ecosystems. Geochemical Perspectives Letters 2016a; In Press

Bagshaw, EA, Tranter, M, Wadham, JL, Fountain, AG and Basagic, H. Dynamic Behaviour of Supraglacial Lakes on Cold Polar Glaciers: Canada Glacier, Mcmurdo Dry Valleys, Antarctica. Journal of Glaciology 2010; 56(196): 366-368

Bagshaw, EA, Wadham, JL, Tranter, M, Perkins, R, Morgan, A, Williamson, CJ, Fountain, AG, Fitzsimons, S and Dubnick, A. Response of Antarctic Cryoconite Microbial Communities to Light. Fems Microbiology Ecology 2016b; 92(6) doi: 10.1093/femsec/fiw076

Bebout, BM, and Garcia-Pichel F. UVB-induced vertical migrations of cyanobacteria in a microbial mat. Applied and Environmental Microbiology 1995; 61: 4215-4222.

Benning, LG, Anesio, AM, Lutz, S and Tranter, M. Biological Impact on Greenland's Albedo. Nature Geoscience 2014; 7(10): 691-691

Campbell, D, Öquist, G. Predicting Light Acclimation in Cyanobacteria from Nonphotochemical Quenching of Photosystem I I Fluorescence, Which Reflects State Transitions in These Organisms. Plant Physiol. (1996) 11 1: 1293-1298

Campbell, D, Hurry, V, Clarke, AK, Gustafsson, Öquist, G. Chlorophyll fluorescence analysis of cyanobacterial photosynthesis and acclimation. Microbiol Mol Biol Rev. 1998: 62(3):667-83

Cameron, KA, Hodson, AJ and Osborn, AM. Structure and Diversity of Bacterial, Eukaryotic and Archaeal Communities in Glacial Cryoconite Holes from the Arctic and the Antarctic. Fems Microbiology Ecology 2012; 82(2): 254-267 doi: 10.1111/j.1574-6941.2011.01277.x

Cartaxana, P, Ruivo, M, Hubas, C, Davidson, I, Serôdio, J, Jesus, B. Light and O2 microenvironments in two contratsing diatom-dominated coastal sediments. Mar. Ecol. Prog. Ser. 2011; 545: 35-47

Chandler, DM, Alcock, JD, Wadham, JL, Mackie, SL and Telling, J. Seasonal Changes of Ice Surface Characteristics and Productivity in the Ablation Zone of the Greenland Ice Sheet. Cryosphere 2015; 9(2): 487-504 doi: 10.5194/tc-9-487-2015

Consalvey MC, Jesus B, Perkins RG, Brotas V, Underwood GJC, Paterson DM. Monitoring migration and measuring biomass in benthic biofilms: the effects of dark/far-red adaptation and vertical migration on fluorescence measurements. Photosynth Res. 2004; 81:91–101

Consalvey, MC, Perkins RG, Paterson DM, Underwood GJC. PAM Fluorescence: A beginners guide for benthic diatomists. Diatom Res. 2005; 20:1–22

Cook, JM, Hodson, AJ, Anesio, AM, Hanna, E, Yallop, M, Stibal, M, Telling, J and Huybrechts, P. An Improved Estimate of Microbially Mediated Carbon Fluxes from the Greenland Ice Sheet. Journal of Glaciology 2012; 58(212): 1098-1108 doi: 10.3189/2012JoG12J001

Dieser, M, Greenwood, M and Foreman, CM. Carotenoid Pigmentation in Antarctic Heterotrophic Bacteria as a Strategy to Withstand Environmental Stresses. Arctic Antarctic and Alpine Research 2010; 42(4): 396-405 doi: 10.1657/1938-4246-42.4.396

Edwards, A, Mur, LAJ, Girdwood, SE, Anesio, AM, Stibal, M, Rassner, SME, Hell, K, Pachebat, JA, Post, B, Bussell, JS, Cameron, SJS, Griffith, GW, Hodson, AJ and Sattler, B. Coupled Cryoconite Ecosystem Structure-Function Relationships Are Revealed by Comparing Bacterial Communities in Alpine and Arctic Glaciers. Fems Microbiology Ecology 2014; 89(2): 222-237 doi: 10.1111/1574-6941.12283

Etzelmüller, B, Schuler, TV, Isaksen, K, Christiansen, HH, Farbrot, H and Benestad, R. Modeling the temperature evolution of Svalbard permafrost during the 20th and 21st century. The Cryosphere 2011; 5, 67–79.

Forster, RM, Kromkamp, JC. Modelling the effects of chlorophyll fluorescence from subsurface layers on photosynthetic efficiency measurement in microphytobenthic algae. Marine Ecology-Progress Series 2004; 284:9-22

Foreman, CM, Wolf, CF and Priscu, JC. Impact of Episodic Warming Events on the Physical, Chemical and Biological Relationships of Lakes in the Mcmurdo Dry Valleys, Antarctica. Aquatic Geochemistry 2004; 10(3): 239-268

Hammer, Ø, Harper, DAT, and Ryan, PD. PAST: Paleontological Statistics Software Package for Education and Data Analysis. Palaeontologia Electronica 2001; 4(1): 9pp.

Hodson, A, Anesio, AM, Ng, F, Watson, R, Quirk, J, Irvine-Fynn, T, Dye, A, Clark, C, McCloy, P, Kohler, J and Sattler, B. A Glacier Respires: Quantifying the Distribution and Respiration Co2 Flux of Cryoconite across an Entire Arctic Supraglacial Ecosystem. Journal of Geophysical Research-Biogeosciences 2007; 112(G4) doi: G04s3610.1029/2007jg000452

Hodson, A, Cameron, K, Boggild, C, Irvine-Fynn, T, Langford, H, Pearce, D and Banwart, S. The Structure, Biological Activity and Biogeochemistry of Cryoconite Aggregates Upon an Arctic Valley Glacier: Longyearbreen, Svalbard. Journal of Glaciology 2010; 56(196): 349-362

Ihnken S, Kromkamp J, Beardall J, Silsbe G. State-transitions facilitate robust quantum yields and cause an over-estimation of electron transport in Dunaliella tertiolecta cells held at the CO2 compensation point and re-supplied with DIC. Photosynthesis Research 2014; 119:257-272

Irvine-Fynn, TDL, Bridge, JW and Hodson, AJ. In Situ Quantification of Supraglacial Cryoconite Morphodynamics Using Time-Lapse Imaging: An Example from Svalbard. Journal of Glaciology 2011; 57(204): 651-657

Kaczmarek, L, Jakubowska, N, Celewicz-Goldyn, S and Zawierucha, K. The Microorganisms of Cryoconite Holes (Algae, Archaea, Bacteria, Cyanobacteria, Fungi, and Protista): A Review. Polar Record 2016; 52(2): 176-203 doi: 10.1017/s0032247415000637

Kromkamp J, Barranguet C, Peene J. Determination of microphytobenthos PSII quantum efficiency and photosynthetic activity by means of variable chlorophyll fluorescence. Mar. Ecol. Prog. Ser. 1998; 162:45–55

Larsson, S. Geomorphological effects on the slopes of Longyear Valley, Spitsbergen, after a heavy rainstorm in July 1972. Geogr. Ann. 1982; 64A: 105 - 125

Langford, HJ, Hodson, A and Banwart, S. Using Ftir Spectroscopy to Characterise the Soil Mineralogy and Geochemistry of Cryoconite from Aldegondabreen Glacier, Svalbard. Applied Geochemistry 2011; 26: S206-S209 doi: 10.1016/j.apgeochem.2011.03.105

Langford, HJ, Hodson, A, Banwart, S and Boggild, C. The Microstructure and Biogeochemistry of Arctic Cryoconite Granules. Annals of Glaciology 2010; 51(56): 87-94

Langford, HJ, Irvine-Fynn, TDL, Edwards, A, Banwart, SA and Hodson, AJ. A Spatial Investigation of the Environmental Controls over Cryoconite Aggregation on Longyearbreen Glacier, Svalbard. Biogeosciences 2014; 11(19): 5365-5380 doi: 10.5194/bg-11-5365-2014

Lavaud, J and Goss, R. The Peculiar Features of Non-Photochemical Fluorescence Quenching in Diatoms and Brown Algae. Advances in Photosynthesis and Respiration 2014; 40: 421-443

Lavaud, J and Lepetit, B. An explanation for the inter-species variability of the photoprotective and non-photochemical chlorophyll fluorescence quenching in diatoms. Biochim. Biophys. Acta 2013; 1827: 294-302

Lawson, EC, Wadham, JL, Tranter, M, Stibal, M, Lis, GP, Butler, CEH, Laybourn-Parry, J, Nienow, P, Chandler, D and Dewsbury, P. Greenland Ice Sheet Exports Labile Organic Carbon to the Arctic Oceans. Biogeosciences 2014; 11(14): 4015-4028 doi: 10.5194/bg-11-4015-2014

Lutz, S, Anesio, AM, Villar, SEJ. and Benning, LG. Variations of Algal Communities Cause Darkening of a Greenland Glacier. Fems Microbiology Ecology 2014; 89(2): 402-414 doi: 10.1111/1574-6941.12351

McMinn A, Ryan KG, Ralph P, Pankowski A. Spring sea ice photosynthesis, primary productivity and biomass distribution in eastern Antarctica, 2002–2004. Mar. Biol. 2007; 151:985–995

Musilova, M, Tranter, M, Bamber, JL, Takeuchi, N and Anesio, A. Experimental Evidence That Microbial Activity Lowers the Albedo of Glaciers. Geochemical Perspectives Letters 2016; 2(0): 106-116 oi: http://dx.doi.org/10.7185/geochemlet.1611

Perkins, RG , Oxborough, K, Hanlon, ARM, Underwood, GJC and Baker, NR. Can chlorophyll fluorescence be used to estimate the rate of photosynthetic electron transport within microphytobenthic biofilms? Mar. Ecol. Prog. Ser. 2002; 228: 47 - 56

Perkins, RG, Mouget, J-L, Lefebvre, S and Lavaud, J. Light response curve methodology and possible implications in the application of chlorophyll fluorescence to benthic diatoms. Mar. Biol. 2006; 149: 703 - 712.

Perkins, RG, Kromkamp. JC, Serôdio, J, Lavaud, J, Jesus, B, Mouget, J-L, Lefebvre, S, Forster, RM. The application of variable chlorophyll fluorescence to microphytobenthic biofilms. In Chlorophyll a fluorescence in aquatic sciences: methods and applications, Edited by Suggett, D., Prasil O., & Borowitzka M. Developments in Applied Phycology 2010a; Vol 4: 237-275. Springer, UK. ISBN 978-90-481-9267-0.

Perkins, RG, Lavaud, J, Serôdio, J, Mouget, J-L, Cartaxana, P, Rosa, P, Barille, L, Brotas, V, Jesus, BM. Vertical cell movement is a primary response of intertidal benthic biofilms to increasing light dose. Mar. Ecol. Prog. Ser. 2010b; 16: 93-103

Remias, D, Pichrtová, M, Pangratz, M, Lütz, C and Holzinger, A. Secondary Pigments and Ultrastructure of Chlainomonas Sp. (Chlorophyta) from the European Alps Compared with Chlamydomonas Nivalis Forming Red Snow. Fems Microbiology Ecology 2016; 92(4) doi: 10.1093/femsec/fiw030

Segawa, T, Ishii, S, Ohte, N, Akiyoshi, A, Yamada, A, Maruyama, F, Li, ZQ, Hongoh, Y and Takeuchi, N. The Nitrogen Cycle in Cryoconites: Naturally Occurring Nitrification-Denitrification Granules on a Glacier. Environmental Microbiology 2014; 16(10): 3250-3262 doi: 10.1111/1462-2920.12543

Serôdio J. Analysis of variable chlorophyll fluorescence in microphytobenthos assemblages: implications of the use of depth-integrated measurements. Aquat Microb Ecol 2004; 36:137–152

Stibal, M, Elster, J, Šabacká, M and Kaštovská, K. Seasonal and Diel Changes in Photosynthetic Activity of the Snow Alga Chlamydomonas Nivalis (Chlorophyceae) from Svalbard Determined by Pulse Amplitude Modulation Fluorometry. Fems Microbiology Ecology 2007; 59(2): 265-273 doi: 10.1111/j.1574-6941.2006.00264.x

Stibal, M, Sabacka, M and Kastovska, K. Microbial Communities on Glacier Surfaces in Svalbard: Impact of Physical and Chemical Properties on Abundance and Structure of Cyanobacteria and Algae. Microbial Ecology 2006; 52(4): 644-654

Takeuchi, N. Optical Characteristics of Cryoconite (Surface Dust) on Glaciers: The Relationship between Light Absorbency and the Property of Organic Matter Contained in the Cryoconite. Annals of Glaciology 2002a; 32: 409-414

Takeuchi, N. Surface Albedo and Characteristics of Cryoconite (Biogenic Dust) on an Alaskan Glacier, Gulkana in the Alaska Range. Bulletin of Glaciological Research 2002b; 19: 63-70

Takeuchi, N, Kohshima, S and Seko, K. Structure, Formation, and Darkening Process of Albedo-Reducing Material (Cryoconite) on a Himalayan Glacier: A Granular Algal Mat Growing on the Glacier. Arctic Antarctic and Alpine Research 2001; 33(2): 115-122

Tedesco, M, Doherty, S, Fettweis, X, Alexander, P, Jeyaratnam, J and Stroeve, J. The Darkening of the Greenland Ice Sheet: Trends, Drivers, and Projections (1981-2100). Cryosphere 2016; 10(2): 477-496 doi: 10.5194/tc-10-477-2016

Van Heukelem, L and Thomas, CS. Computer-assisted high-performance liquid chromatography method development with applications to the isolation and analysis of phytoplankton pigments. Journal of Chromatography A 2010; 910: 31 49

Yallop, ML and Anesio, AM. Benthic Diatom Flora in Supraglacial Habitats: A Generic-Level Comparison. Annals of Glaciology 2010; 51(56): 15-22 doi: 10.3189/172756411795932029

Yallop, ML, Anesio, AM, Perkins, RG, Cook, J, Telling, J, Fagan, D, MacFarlane, J, Stibal, M, Barker, G, Bellas, C, Hodson, A, Tranter, M, Wadham, J and Roberts, NW. Photophysiology and Albedo-Changing Potential of the Ice Algal Community on the Surface of the Greenland Ice Sheet. Isme Journal 2012; 6(12): 2302-2313 doi: 10.1038/ismej.2012.107

Zarsky, JD, Stibal, M, Hodson, A, Sattler, B, Schostag, M, Hansen, LH, Jacobsen, CS and Psenner, R. Large Cryoconite Aggregates on a Svalbard Glacier Support a Diverse Microbial Community Including Ammonia-Oxidizing Archaea. Environmental Research Letters 2013; 8(3) doi: 10.1088/1748-9326/8/3/035044

Zawierucha, K, Kolicka, M, Takeuchi, N and Kaczmarek, L. What Animals Can Live in Cryoconite Holes? A Faunal Review. Journal of Zoology 2015; 295(3): 159-169 doi: 10.1111/jzo.12195

Table 1. Species Composition of Cryoconite Material (pooled for three cryoconite holes)

Cyanophyta	Chlorophyta	Streptophyta	Chromophyta
Leptolynbya spp. *Nostoc* spp. *Oscillatoria* spp. *Pseudoanabaena* spp.	*Chlamydomonas* cf. *nivalis* *Chlamydomonas spp.*	*Ancylonema nordenskiöldii* *Cylindrocystis brebissonii* *Mesotaenium berggrenii*	Pennate diatom spp.

Table 2. Concentration of pigments quantified in by HPLC. Values are given as µg.g^{-1} freeze-dried cryoconite material.

	Hole 1	**Hole 2**	**Hole 3**
FUCO (Fucoxanthin)	0.0464	0.0000	0.0513
NEOX (Neoxanthin)	0.0917	0.0000	0.0227
VX (Violaxanthin)	0.1180	0.0141	0.0408
DDX (Diadinoxanthin)	0.0602	0.0275	0.0250
ZX (Zeaxanthin)	0.0543	0.0000	0.0000
LUT (Lutein)	0.6769	0.0176	0.0635
CANT (Canthaxanthin)	0.4924	1.1182	0.6538
CHLB (Chlorophyll b)	1.3474	0.4198	0.0801
ECHI (Echinenone)	0.6267	0.1702	0.2387
CHLA (Chlorophyll a)	10.6670	6.1472	5.4459
CART (Carotenoids)	0.3431	0.0000	0.0622

Table 3. Pigment ratios relative to Chlorophyll a. For abbreviations, see Table 2.

	Site 1	**Site 2**	**Site 3**
FUCO	0.0044	0.0000	0.0094
NEOX	0.0086	0.0000	0.0042
VX	0.0111	0.0023	0.0075
DDX	0.0056	0.0045	0.0046
ZX	0.0051	0.0000	0.0000
LUT	0.0635	0.0029	0.0117
CANT	0.0462	0.1819	0.1200
CHLB	0.1263	0.0683	0.0147
ECHI	0.0588	0.0277	0.0438
CART	0.0322	0.0000	0.0114

Figure 1. Location of sampling and *in situ* fluorescence measurements (blue dot) on the surface of Longyearbreen, Spitsbergen, Svalbard. Samples were collected from clean ice with intermittent cryoconite coverage, away from adjacent to areas with high concentrations of surface debris (upper insert, lower blue triangle) and meltwater channels (lower insert, upper blue triangle).

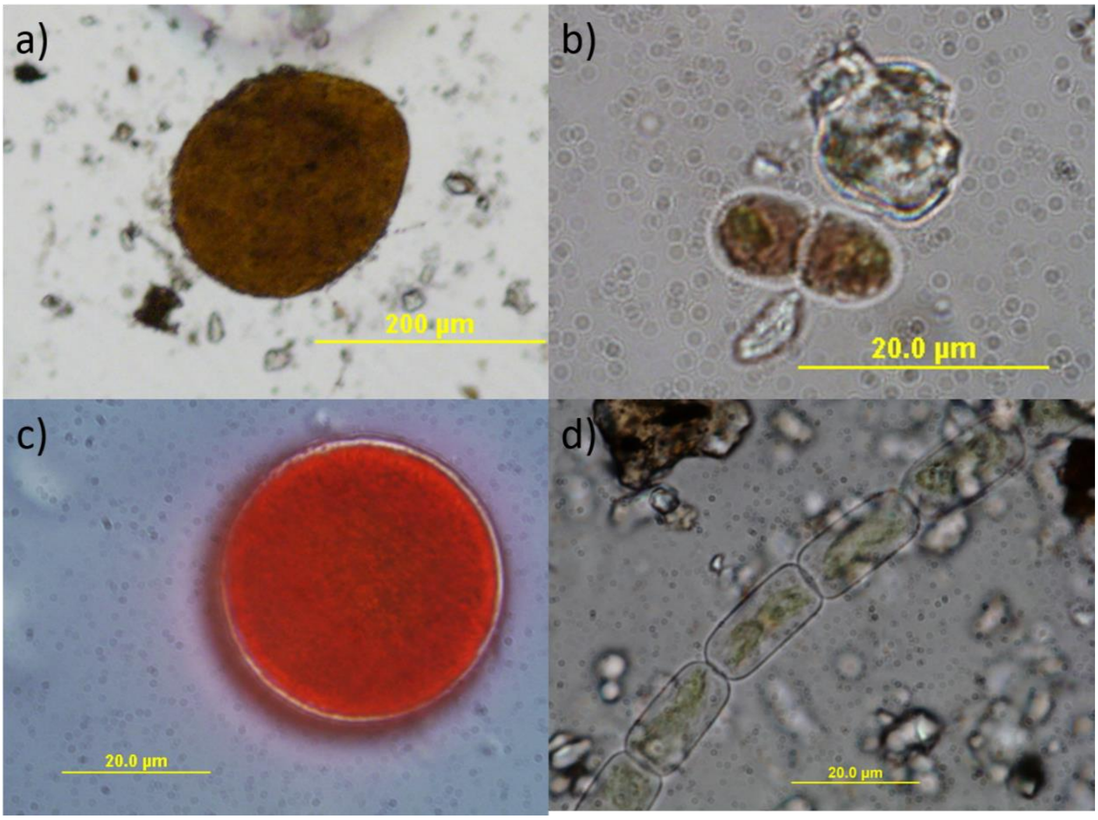

Figure 2. Cyanobacteria and algae from Longyearbreen cryconite: a) *Nostoc* sp. colony; b) Dividing cells of *Mesotaenium berggrenii*; c) Zygospore of *Chlamydomonas* cf. *nivalis*; d) Filament of *Ancylonema nordenskiolldii.*

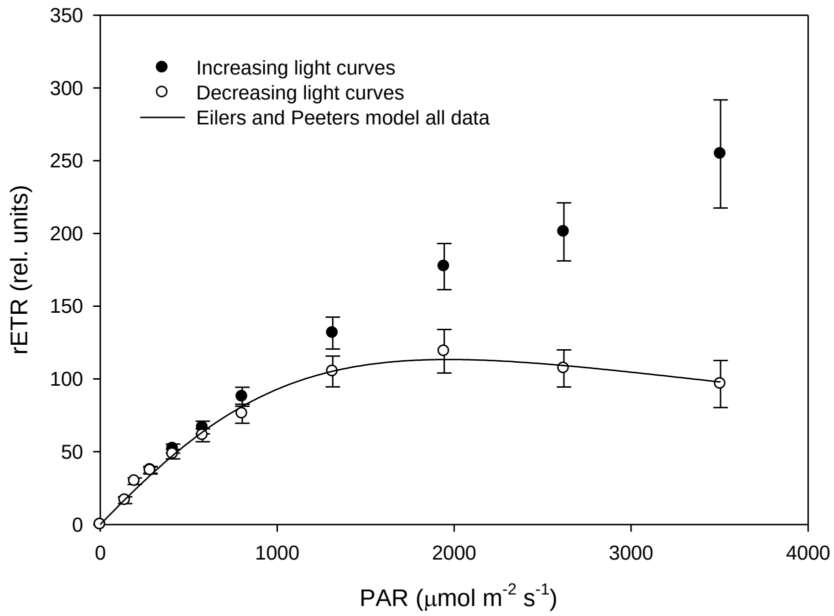

Figure 3. Increasing rapid light curve (RLC) data (closed symbols, mean ± s.e., n = 15) showing no saturation in comparison with decreasing RLC data (open symbols, mean ± s.e., n = 15) showing saturated light curves. Fitted line is the Eilers and Peeters (1988) model regressed to the 15 replicate curves data points. Increasing and decreasing light curves were carried out on separate samples each time and with sequentially increasing or decreasing light levels steps respectively.

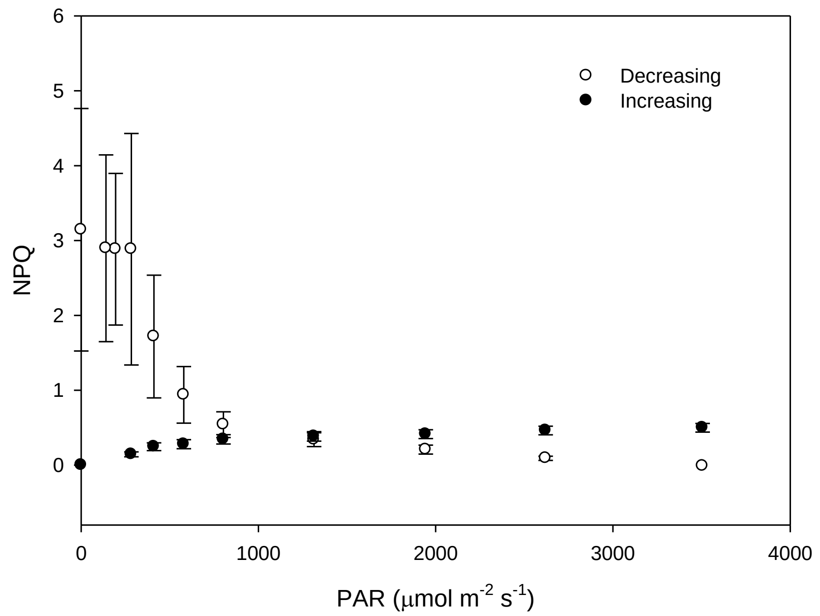

Figure 4. Increasing rapid light curve (RLC) non-photochemical quenching (NPQ) data (closed symbols, mean ± s.e., n = 15) and decreasing RLC NPQ data (open symbols, mean ± s.e., n = 15) for the light curves shown in Figure 3. Increasing and decreasing light curves were carried out on separate samples each time and with sequentially increasing or decreasing light levels steps respectively.

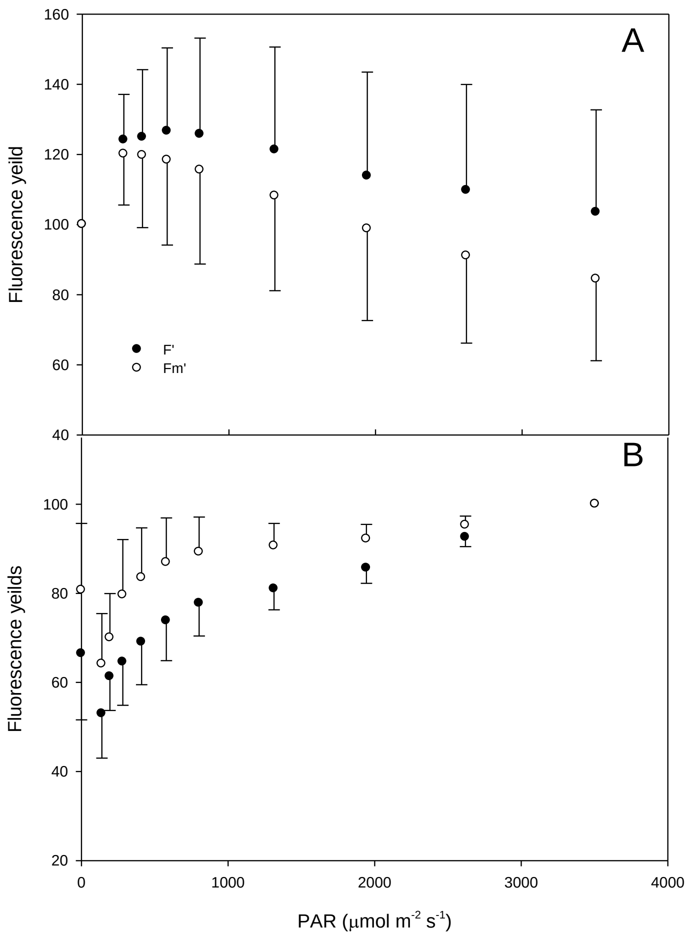

Figure 5. Operational fluorescence yield (*F'*, closed symbols) and maximum fluorescence yield (F_m', open symbols) yield for increasing (a) and decreasing (b) rapid light curves shown in Figure 1 (both data sets mean ± s.e., n = 15). Data are represented as the percentage of the initial values obtained from the first light curve step in each case (hence 100% at 0 μmol m^{-2} s^{-1} for increasing and 100% at 3,600 μmol m^{-2} s^{-1} PAR for decreasing light curve steps).

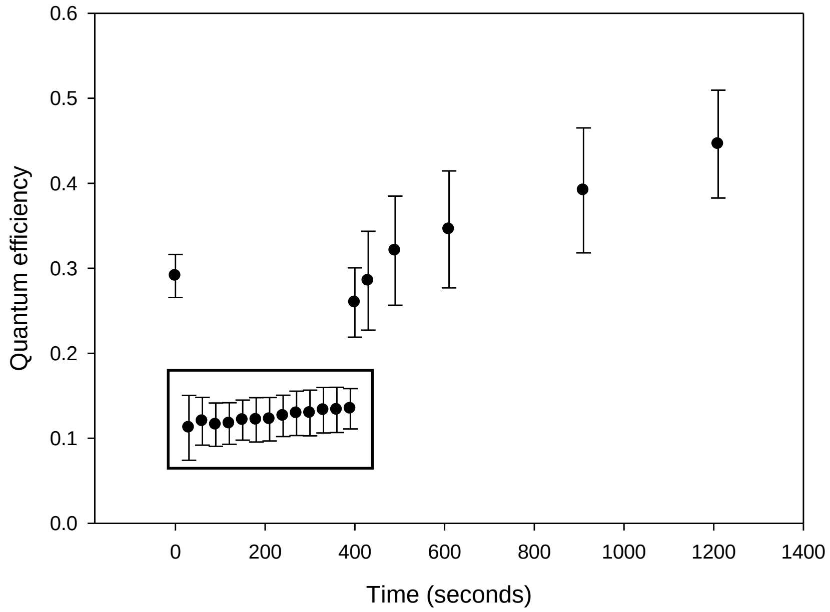

Figure 6. Quantum efficiency during induction recovery curve measurements (mean ± s.e., n = 8). The boxed area shows the efficiency during the induction phase with applied actinic light, other data points are in darkness.

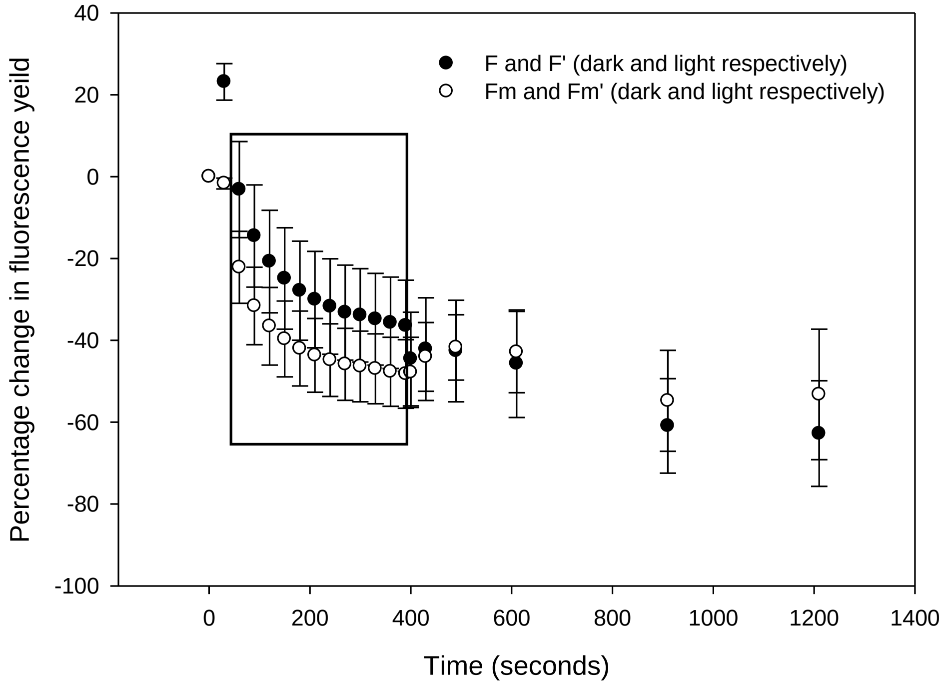

Figure 7. Percentage change, relative to initial values, of the operational fluorescence yield (*F* and *F'* in the dark and light respectively) and maximum fluorescence yield (F_m and F_m' respectively) during induction recovery curves (mean ± s.e., n = 8). The boxed area shows the yields measured during the induction phase with applied actinic light, other data points are in darkness.